Applied Physics 50, 445501 (2017)

Thermal management approaches of $Cu(In_x,Ga_{1-x})Se_2$ micro-solar cells

Diego Sancho-Martínez[1], Martina Schmid[1,2]

[1]*Nanooptical Concepts for Chalcopyrite Solar Cells, Helmholtz-Zentrum Berlin, Hahn-Meitner-Platz 1, 14109 Berlin, Germany*

[2]*Experimental Physics, Faculty of Physics, University of Duisburg-Essen, Lotharstr. 1, 47057 Duissburg, Germany*

Abstract

Concentrator Photovoltaics (CPV) is a cost-effective method for generating electricity in regions that have a large fraction of direct solar radiation. With the help of lenses, sunlight is concentrated onto miniature, highly efficient multi-junction solar cells with a photovoltaic performance above 40%. To ensure illumination with direct radiation, CPV modules must be installed on trackers to follow the sun's path. However, the costs of huge concentration optics and the photovoltaic technology used, narrow the market possibilities for CPV technology. Efforts to reduce these costs are being undertaken by the promotion of $Cu(In_x,Ga_{1-x})Se_2$ solar cells to take over the high cost multi-junction solar cells and implementing more compact devices by minimization of solar cell area. Micrometer-sized absorbers have potential of low cost, high efficiencies and good thermal dissipation under concentrated illumination. Heat dissipation at low (<10x) to medium (10x to 100x) flux density distributions is the key point of high concentration studies for macro- and micro-sized solar cells (from 1 μm^2 to 1 mm^2). To study this thermal process and to optimize it, critical parameters must be taken in account: absorber area, substrate area and thickness, structure design, heat transfer mechanism, concentration factor and illumination profile. A close study on them will be carried out to determine the best structure to enhance and reach the highest possible thermal management pointing to an efficiency improvement.

1. Introduction

Recently, $Cu(In_x,Ga_{1-x})Se_2$ (CIGSe) solar cells were given a boost reaching even higher efficiencies, exceeding the 22.6% efficiency mark under indoor laboratory measurements by ZSW [1]. CIGSe solar cells rely on materials of limited availability such as In or Ga, which can be reduced by decreasing the amount of indium in the solar cell, approaching a wide band-gap energy material with lower efficiencies in comparison with referenced CIGSe solar cells [2] [3]. Indium and gallium can also be diminished by the reduction of the absorber thickness, leading to increased optical losses due to reduced light absorption. However, this drawback can be resolved by the introduction of nanostructures [4] [5]. Plasmonic or dielectric nanostructures are used as reflectors, antennas or light trapping devices to redirect light into the absorbing medium enhancing the solar cell performance. A third scenario to reduce the amount of In and Ga is the minimization of solar cell area, i.e. CIGSe micro solar cells combined with optical elements to concentrate sun radiation. Micro-cells

offer higher efficiencies than conventional designs, whilst scarce elements like In and Ga are reduced. Proofs of concept using micro-sized CIGSe solar cells and an optical system adapted to concentrate light in photovoltaic systems with low (LCPV: <10x) and medium (MCPV: 10x to 100x) concentration factor have been given before [6] [7] [8] [9] [10]. Light concentration induces a logarithmic increase of the open circuit voltage (V_{oc}) and a linear development of the short circuit current (I_{sc}) of the cell, but the performance is reduced by the cell temperature increasing with concentration. The temperature is therefore a critical parameter for adjusting the maximum possible concentration flux without diminishing the output performance of the device [11] [12].

Micro-sized solar cells require improved heat dissipation and a more compact module design compared to macroscopic concentrators. To determinate the maximum possible concentration factor without damaging the cell, a thermal study of a micro-sized cell (from 1 μm^2 to 1 mm^2) will be presented. The PV cell temperature behavior will be analyzed under different conditions and concentration factors using finite element analysis software [13].

2. Simulations details

The temperature profile of the solar cell is simulated as a function of energy irradiance (flux and spatial distribution). PV cell design specifications will be considered as free parameters of the simulation: thermal efficiency of the photovoltaic system is studied comparing different structures (substrate thickness, back contact thickness, substrate area, etc.) to enhance solar cell heat dissipation leading to an efficiency improvement.

Each element has a contribution on the final temperature of the solar cell, thus modeling started with the simplest scenario, and its complexity was gradually increased. Figure 1a represents schematically the device used in modeling. The basic structure consists only of one p-type absorber and a back contact layer deposited on soda lime glass (SLG) substrate. This structure is stacked on a chuck kept at room temperature (20°C) to dissipate the undesired heat of the PV device without considering thermal losses at this interface, the error without including loses in the active cooling is a 0.3%. For this ideal case structure, the characteristics used for the layers are according to photovoltaic large scale industry: a 3 mm thick soda-lime glass substrate [14], an 800 nm thick Mo layer [15] [16] [17] and a 2 μm CIGSe absorber layer [18]. Buffer (CdS) and front contact (i-ZnO/AZO) layers are overlooked.

A more complex scenario is subsequently considered and figure 1b represents this more realistic situation. Here, the ideal structure is encapsulated with a 1 mm thick borosilicate cover glass (BSG) or lens (plastic or BSG) array for protection against environmental conditions (mainly humidity) and for light concentration. A 50 nm thick n-type (CdS) layer and a 450 nm thick front contact (i-ZnO/AZO) sheet are included. For the realistic case, no active cooling was induced and conduction, convection and radiative heat transfer mechanism are considered in the simulations.

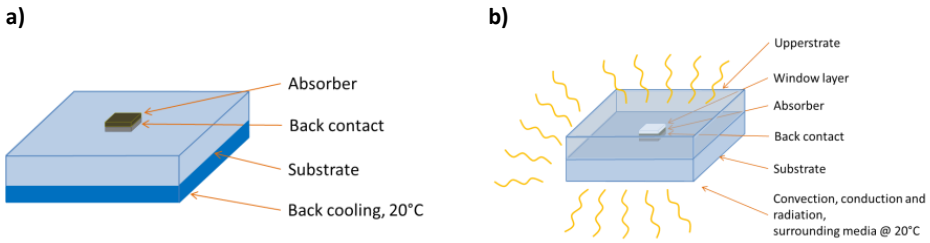

Figure 1: 3D sketch of the solar device; **(a)** ideal case: basic structure with active cooling (rear side at 20°C), **(b)** realistic case: solar module without active cooling but with fundamental heat transfer mechanisms (convection, conduction and radiative heat dissipation to surrounding media at 20°C).

Parameters modified during simulations are: substrate thickness, back contact thickness, substrate area, back contact area, absorber area and back contact material, in the ideal case structure and a comparison to the realistic case structure. The cell temperature behavior for those parameters will be determined as a function of the concentration factor which is given by the ratio between substrate and cell area, assuming that the whole incoming light could be concentrated without losses. The concentration factor *C* therefore is defined as follows:

$$C = \frac{Area_{substrate}}{Area_{solar\ cell}} \quad [1]$$

where $Area_{substrate}$ and $Area_{solar\ cell}$ are the substrate and solar cell area, respectively. Hence, final solar cell irradiance will be defined as the concentration factor multiplied by the sun irradiance (1000 W/m^2).

In this paper, partial absorption and conversion to heat of the AM1.5 spectrum at the pn-junction is assumed. Reflection between different medium will be included. The reflected power for Air/AZO, Air/BSG, BSG/AZO, AZO/CIGSe and CIGSe/Mo is 8.2%, 4.0%, 0.8%, 6.3% and 1.2% of the incoming light, respectively. The total reflection used for the basic study and for the realistic one is 13.2% and 9.9%, respectively. The CIGSe absorber band gap (from 1.04 to 1.68 eV depending on the Ga content [3]) will determine the amount of energy absorbed by the solar cell. GDOES characterization of our fabricated solar cells shows a band gap of 1.185 eV, which we assume in our calculations. Sub-band gap energy photons and UV light will not be absorbed completely [19], 10.2% and 7.7% of the incoming power will not contribute to heat generation, respectively. Non-absorbed light will travel through the PV device without contributing to power generation. The maximum irradiance absorption of the solar cell based on its spectral response and the sun spectrum will be 819 W/m^2. Power conversion to electricity will be taken into account in this study; a 16% efficiency conversion will be used in the simulations. Joule heating produced by the cell performance is considered in the simulations. Including the light absorption and conversion to electricity of the solar cell, the incoming power on the device will be diminished by the cell efficiency and the ohmic heating will be increased with the cell current. We have seen experimentally that the joule heating power is below 3% of the incoming power as it is decreasing the series resistance (R_s) with concentration. The current of the PV cell increases linearly with concentration and the logarithm of the series resistance drops linearly with the logarithm of the concentration [10]. The maximum cell temperature will be analyzed for different

concentration factors supported by prior hypotheses. The reference irradiance used for the basic case and for the realistic one taking into account the total light reflection, non-absorbed photons, the power conversion to electricity and Joule heating will be 600 W/m^2 and 620 W/m^2, respectively.

Thermal properties used for the different materials are summarized in Table 1. The fundamental heat transfer modes conduction, convection and radiation (CCR) are employed. Conduction was applied considering a perfect back cooling device for the ideal structure, which was kept at 20°C. CCR heat dissipation mechanisms were all used in the realistic case study, where as a boundary condition the surrounding air was set to 20°C (standard test conditions) and no active cooling was implemented.

Table 1:
Material properties used for the modeling [13] [20] [21]

Parameter	Units	Substrate	Back contact	CIGSe	Buffer layer	Front contact	Upperstrate
Size	mm^2	1 x 1		10^{-6} to 1			1 x 1
Thickness	nm	$3{\cdot}10^6$	800	$2{\cdot}10^3$	50	450	$1{\cdot}10^6$
Emissivity	-	0.87	Mo 0.2	0.87	0.87	0.87	0.87
Thermal conductivity	W/(m·K)	1.4	Mo 250 Cu 400	5	5	50	1.4
Heat capacity	J/(kg·K)	730	Mo 138 Cu 385	325	325	505	730
Convective heat transfer coefficient	W/(m·K)	10.45	-	-	-	-	10.45

Equations used by the finite element software employed (COMSOL [13]) for conductive heat transfer, surface-to-ambient radiative heat transfer, convective heat transfer and boundary conditions are as follows [22]. Conductive heat transfer equation:

$$\rho \cdot C_p \cdot \frac{\partial T}{\partial t} + \nabla \cdot (-k \cdot \nabla T) = Q \quad [2]$$

where T is the solar cell temperature, $\boldsymbol{\rho}$ is the material density, C_p and k represent heat capacity and thermal conductivity, respectively, and Q is the heat source energy. The surface-to-ambient radiation heat transfer equation:

$$\varepsilon \cdot \sigma \cdot \left(T_{amb}^4 - T^4\right) = q \quad [3]$$

where T and T_{amb} are the solar cell and ambient temperature, respectively. ε and σ represent emissivity and Stefan-Boltzmann constant, respectively, and q is the heat flux. The convective heat transfer equation:

$$h \cdot (T_{amb} - T) = q_0 \quad [4]$$

where T and T_{amb} are solar cell and surrounding temperature, h represents the conductive heat transfer and q_0 is the inward heat flux. A common type of heat flux boundary conditions is the one where T_{amb} is the temperature far away from the modeled domain and the heat transfer coefficient, h, represents all the physics occurring between the boundary and these "far regions". The most common situation is that h is referred to as conductive heat transfer. The boundary conditions of the simulation domain fulfill the equation:

$$-\boldsymbol{n} \cdot \boldsymbol{q} = q_0 \quad [5]$$

where $\boldsymbol{n}$ is the normal vector of the boundary, $\boldsymbol{q}$ and q_0 represent heat flux vector and inward heat flux, respectively. The heat source is applied on the upper surface of the absorber, CIGSe, and is partially absorbed in this region based on our simulation approaches. A planar heat source (W/m^2) is used instead of a volumetric heat source (W/m^3) at the p-type material. The light beam will lose intensity due to absorption and scattering when the beam passes through the solar cell. The absorption of light will not be homogeneous along the cell [19] and a volumetric heat source therefore is not suitable to be used in this study.

The meshing of the desired structure was employing a maximum element size of 0.14 mm and a minimum element size of 0.006 mm using a free tetrahedral entity for the geometry. For smaller structures, the FEM adapt the structure to fit enough free tetrahedral inside of the layer.

3. Results and Discussion

3.1. Ideal case: study of different substrate thicknesses and back contact properties with active back interface cooling

Different simulations are performed to find the best structure to enhance the solar cell heat dissipation. The first step of the simulations (based on the ideal case structure, figure 1a) consists of modifying the glass substrate thickness to examine the heat development of the solar cell. For each parameter variation, different CIGSe solar cell sizes (from 1 mm down to 1 μm absorber widths) equaling to different concentrations (from 10^0x to 10^6x) are considered.

A reliable solar cell temperature range suitable for CPV applications is below 150°C, and it is even better if the cell operates under 100°C, otherwise the temperature could damage the pn-junction [23] [24].

The maximum cell temperature is increasing as the concentration grows, see figure 2a. Low to high concentration factors, from 10^0x up to 10^5x, lead to cell temperatures below 150°C. Higher concentration values generate a temperature above 150°C to 480°C on the cell at 10^6x (not shown).

In this simulation, back contact and absorber layer have the same area. The molybdenum layer has better conduction properties to dissipate the generated heat on the cell than glass. Nevertheless, undesired heat under high concentration factors cannot be properly dissipated due to the insignificant back contact area and the low substrate thermal conductivity. The solar cell temperature behavior once concentrating light on it is only slightly improved by decreasing the glass thickness because the thermal conductivity remains invariable, 178 times lower than molybdenum. Reducing the distance between cooling device and cell encourages heat dissipation by cause of diminishing the heat gradient paths. Figure 3b shows thermal gradient lines of the ideal solar device, where most of the glass volume is not used to cool down the micro-cell. Short gradient lines are more desirable than long ones to improve the cooling effect on the solar cell.

A limiting factor for a better heat dissipation is the thermal conductivity of glass. Usually, the reduction of cell area goes hand in hand with the decrease of the back contact area. Spreading the heat along the substrate surface would enhance heat management. Using the metal contact for this purpose, the cell thermal management will be investigated for different molybdenum areas under concentrated light. In figure 2b, the cell temperature evolution is analyzed for different light fluxes and cell sizes for a back contact area equal to the cell area and for a molybdenum area which covers the whole substrate (using the same device structure as in the previous case). Thermal simulations increasing back contact area show a significant heat dissipation improvement (figure 2b). The cell temperature drops from 480°C (not shown) to 289°C at 10^6x when the metal area is increased from cell area to entire substrate area. Size increment allows the structure to dissipate properly the generated heat on the cell by reducing the gradient paths, thus improving the PV cooling. High concentration factors, up to $2 \cdot 10^5$x, could be applied on the micro-solar cell, being in a trustworthy temperature range up to 150°C.

A 3D isothermal surface cross section and a zoom in (figure 3a) of the ideal case structure (with a 3 mm glass substrate and a back contact area equal to the cell area) indicate that back contact area gain would encourage heat dissipation due to the heat lateral spreading. Short gradient paths improve the cell temperature cooling better than long ones. In figure 3b, temperature gradient lines for the different views front, side and top are shown, where long gradient lines on the sides of the cell are produced due to the scant lateral glass heat conduction.

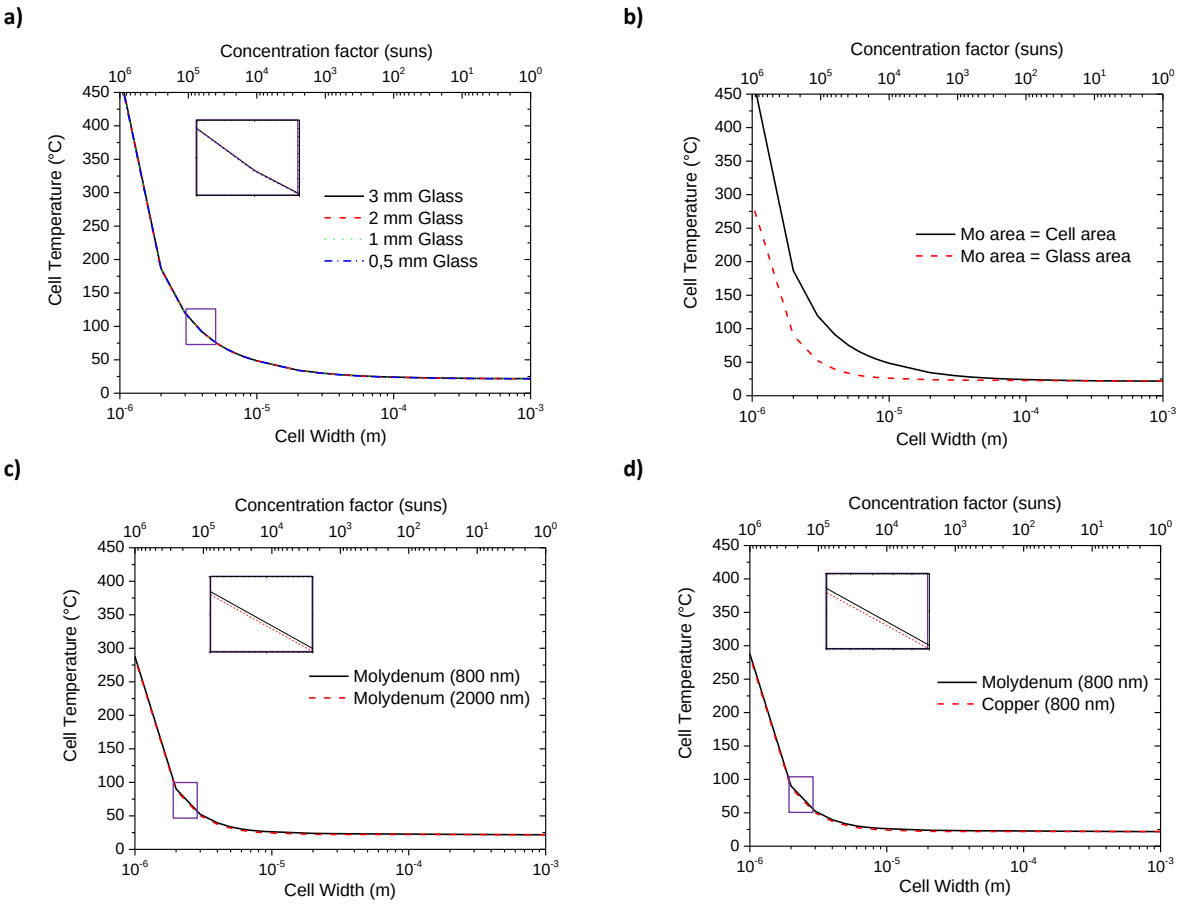

Figure 2: Maximum temperature on CIGSe solar cell under different concentration factors, varying structure parameters and fixing the substrate area (1 mm^2): **(a)** reducing glass thickness (back contact area equal to cell size), **(b)** increasing back contact area, **(c)** increasing back contact thickness (back contact area equal to substrate size), and **(d)** changing back contact material (back contact area equal to substrate size).

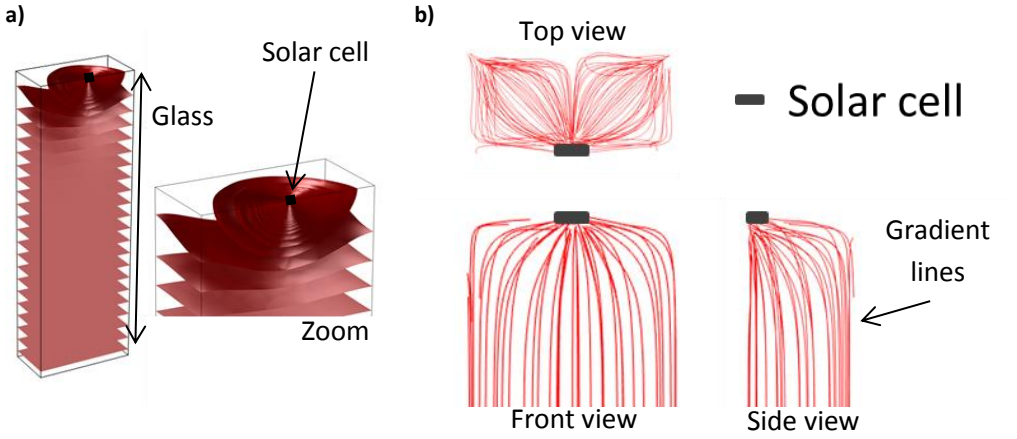

Figure 3: Heat spreading in ideal solar device; **(a)** 3D isothermal cross section and a zoom in, **(b)** thermal gradient lines plotted for different views: side, top and front, for the device structure: a 3 mm thick glass substrate (with an area of 1 mm^2), an 800 nm molybdenum layer and a 2 μm thick CIGSe absorber.

The consequence of expanding back contact area is a superior heat management. For further simulations, the back contact metal always covers the entire substrate area. Augmenting molybdenum thicknesses the temperature behavior of the device may be expected to improve further. A comparison between 800 and 2000 nm back contact thicknesses under different levels of sun concentration originating from different cell sizes is studied. Figure 2c, shows a slight improvement of the final cell temperature with increasing Mo thickness. A thicker metal layer may improve slightly the glass heat dissipation because the heat was already spread along the substrate surface by increasing the Mo area, but a thicker layer could easily be delaminated or detached from the substrate and remove the materials deposited on it [25]. Nonetheless, an even thinner back contact will be sufficient to spread heat along the substrate surface but the electrical properties and the posterior process parameters will reduce its benefits. Therefore, for further studies, the 800 nm thick back contact will be used in our thermal analysis.

The back contact layer area rather than its thickness has demonstrated a high impact on the heat management of the solar cell. Being replaced with a better thermally conductive material might reinforce heat dissipation by extracting the generated heat from the solar cell and spread along the substrate. The new material should resist against a high temperature absorber fabrication process and avoid contamination with undesired impurities. K. Orgassa [26] has investigated different back contact metals, with W and Mo providing the best cell performance due to less absorber/back contact interface passivation and less Se reactivity compared to Cr, Ta, Nb, V, Ti or Mn. Yet, both materials are listed as current supply risk elements [27]. A substitute for molybdenum could be copper, since it has a very low supply risk, it is part of the following production process (absorber formation) and it has better conduction properties compared to molybdenum. The cell temperature behavior is analyzed using the ideal case structure with a Cu back contact over the whole substrate surface for different concentration factors. As a result of improved conduction properties, a slight

improvement of the final cell temperature is achieved as shown in figure 2d. Thicker or better conductive back contacts are equivalent:

$$k \cdot t = const \quad [6]$$

where k represents thermal conductivity and t is the back contact thickness, but do not produce any noticeable improvement in heat due to the substrate thermal properties. Therefore, a better conducting substrate would boost the cooling characteristics.

3.2. Realistic case: study of different cooling approaches and cell-substrate ratios

High concentration CPV systems use active cooling to dissipate the generated heat on the cell due to high light fluxes. This technique requires a complete cooling circuit which increases the final cost of the CPV module. To avoid active cooling, an improved device structure to dissipate heat is needed. To obtain accurate simulation results it is necessary to include the fundamental heat transfer modes. Conduction, convection and radiation (CCR) of heat were implemented in the model. A surrounding material at room temperature was set as boundary condition for radiation and convection modes but not for conduction at the rear interface. A comparison of two scenarios has been investigated: when the device structure has an ideal back cooling system and when the three heat transfer modes are considered instead. A 3 mm thick glass substrate, an 800 nm molybdenum layer (which covers the whole surface) and a 2 μm thick CIGSe absorber are part of the structure. Here a 50 nm thick buffer layer (CdS), a 450 nm thick transparent conductive layer (AZO) and 1 mm thick glass upperstrate are included to simulate a real device, compare figure 1b. The maximum solar cell temperature performance was simulated for different concentration factors for both scenarios. Figure 4 gives the results and reveals that heat dissipation is significantly higher with substrate cooling. In both studies, the maximum cell temperature is below the reported pn-junction breakdown temperature, which usually occurs in the range from 150°C to 225°C [24]. Below these values, the performance of the cell is enhanced by concentrating light but, above 150°C, the solar cell stability is endangered. High concentration (>10^5x) could be used to generate electricity from micro-sized solar cells (<$2 \cdot 10^{-5}$ m), leading to a high material salvage (>10^5x). The cost of CPV devices is reduced exploiting CCR heat mechanisms and avoiding active cooling. A realistic temperature management is given by using CCR modes for non-active cooling systems.

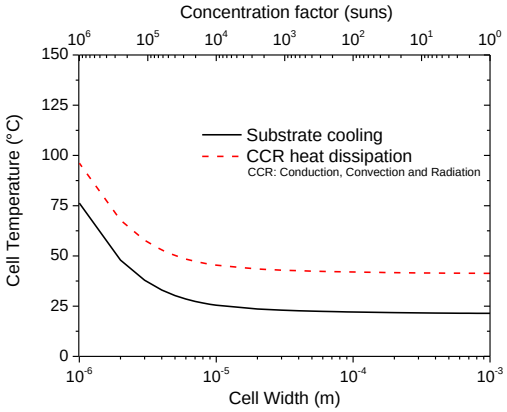

Figure 4: Maximum temperature of CIGSe-solar cell under different concentration factors for different heat dissipation methods: substrate back ideal cooling system and conduction, convection and radiation (CCR) heat transfer mechanism for the device structure: a 3 mm thick glass substrate (with an area of 1 mm^2), an 800 nm molybdenum layer (with an area of 1 mm^2), a 2 μm thick CIGSe absorber, a 50 nm thick buffer layer (CdS), a 450 nm thick transparent conductive layer (AZO) and 1 mm thick glass upperstrate (with an area of 1 mm^2).

Including convection, conduction and radiation heat transfer mechanisms results in higher temperatures in comparison with only active cooling without CCR modes, as displayed in figure 4. Nevertheless, these results are below the critical pn-junction breakdown range. The maximum concentration factor is investigated for the non-ideal case changing cell and substrate sizes. The substrate-cell ratio (as defined in equation 1) provides the effective concentration factor applied in the simulations. Varying the substrate area keeping constant the cell size or changing the cell area preserving substrate size will increase or diminish the irradiation value. An isothermal surface graph is presented in figure 5a, where the maximum cell temperature is displayed for different substrate and cell areas. In figure 5b, an isoconcentration factor map is plotted for the same dependence, to show the concentration distribution (isothermal white lines are superimposed in the same figure).

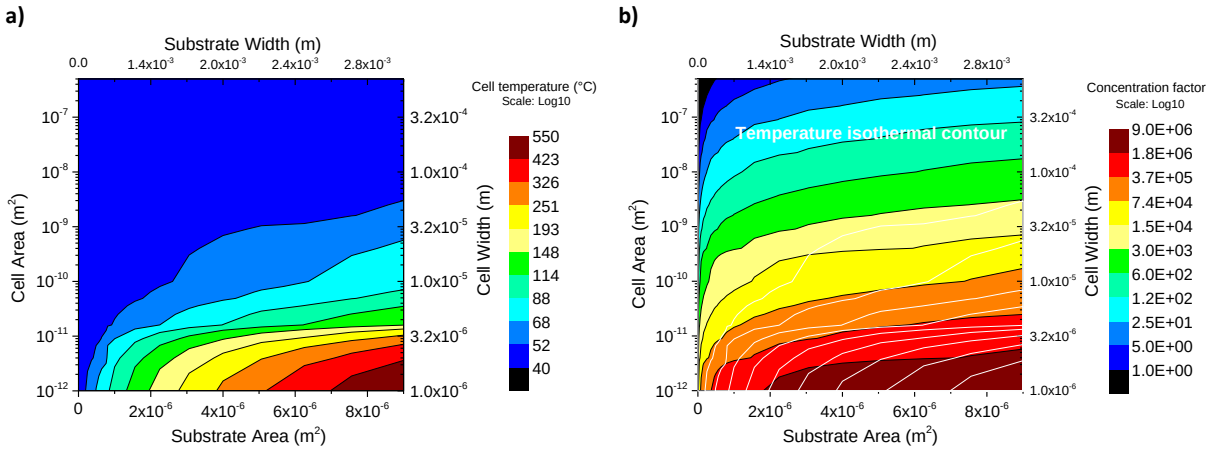

Figure 5: (a) Maximum temperature and **(b)** established concentration factor on CIGSe solar cell changing substrate and cell area ratio (overlapped in white Figure 5a) for the device structure: a 3 mm thick glass substrate (with an area of 1 mm^2), an 800 nm molybdenum layer (with an area of 1 mm^2), a 2 μm thick CIGSe absorber, a 50 nm thick buffer layer (CdS), a 450 nm thick transparent conductive layer (AZO) and 1 mm thick glass upperstrate (with an area of 1 mm^2).

Different concentration factors are applied for each structure, varying substrate width (from 10^{-5} to $3 \cdot 10^{-3}$ m) and solar cell width (from 10^{-6} to 10^{-3} m). Heat dissipation is enhanced using larger substrate and cells lengths, i.e. low concentration factors (from 1x to 10x). Tuning the

glass length to larger values and keeping PV cell size over 10^{-5} m concentration values (figure 5b) grow faster than the maximum cell temperature. In this region, medium to high C values (from 10x to $3.7 \cdot 10^5$x) could be reached, where the device stays in a dependable temperature range below 150°C (figure 5a) suitable for CPV applications. Only for high concentration factors, higher than 10^5x, the cell temperature is above the breakdown lower limit. From here, no ultimate conclusion about the best substrate-cell area ratio could be extracted. Nevertheless, medium to high concentrations (from 10x to $3.7 \cdot 10^5$x) appear feasible as the micrometer-sized solar cells are in a trustworthy temperature operation region. Device fabrication will restrain the minimum CIGSe solar cell size and based on it, substrate dimensions would be selected to obtain the best possible thermal performance.

3.3. Realistic case: study of different illumination profiles

Medium to high concentrations are feasible in micrometer-sized solar cells as we have proved before, due to better heat management compared to macroscopic systems [9]. Efficiency enhancement should go hand in hand with the incorporation of micro-lenses which will concentrate incoming light onto the absorber. Usually, CPV technology employs lenses or mirrors to focus sunlight onto the solar cells [28]. While this allows for more efficient PV energy generation, the use of additional optics for focusing sunlight has also driven up the cost of concentrated photovoltaics compared to conventional photovoltaic devices [29]. Concentrating light, however, employs direct sunlight rather than diffuse light requiring tracking systems [30]. Different technologies are used for concentration, for example: Fresnel lenses, parabolic mirrors, reflectors or luminescent concentrator systems. However, for a cheap device increasing angular tolerance of illumination, simplifying tracking systems, reducing focal length and lowering the number of optical elements is strongly required [28]. Furthermore, a good concentrator system should be able to tolerate misalignment, various irradiation profiles and light spectrum mismatch providing an acceptable performance. CPV optical systems often do not produce a uniform flux density distribution at the output aperture [28]. As an example, Fresnel concentrator lenses produce a Gaussian like light distribution image although not as sharp as the equivalent simple spherical lens due to diffraction at the edges of the ridges [31].

Here we examine the temperature management for different Gaussian beam profiles on a 100 μm diameter micro solar cell including the three fundamental heat dissipation mechanisms (CCR) of the realistic model. Figure 6a shows selected Gaussian beam distributions applied in the simulation. The volume contained below the different Gaussian profiles is implemented to be equal, considering that the solar cell receives the same amount of energy regardless of the shape of the Gaussian beam. The heat management is simulated for a variety of Gaussian standard deviation values from 100 to 0.01 μm, in terms of full width at half maximum (FWHM) from 235 to 0.02 μm ($FWHM = 2 \cdot \sqrt{2 \cdot ln2} \cdot \sigma$).

The maximum cell temperature profile is shown in figure 6b for the incident Gaussian beams plotted in figure 6a. Narrow beam profiles produce highly localized heat onto the cell which could lead to a hot point and produce a shunted cell if the temperature value is above 150°C. Flat irradiation profiles are desirables for heat dissipation and lower cell temperatures as the simulations depicted. But higher design tolerances are provided using narrow Gaussian beams helping to simplify tracking systems or to mitigate the effect of lens misalignment. Even for tiny FWHM values (< 0.1 μm), the maximum cell temperature remains below 100°C boosting the cell tolerance against focusing elements.

a)

b)

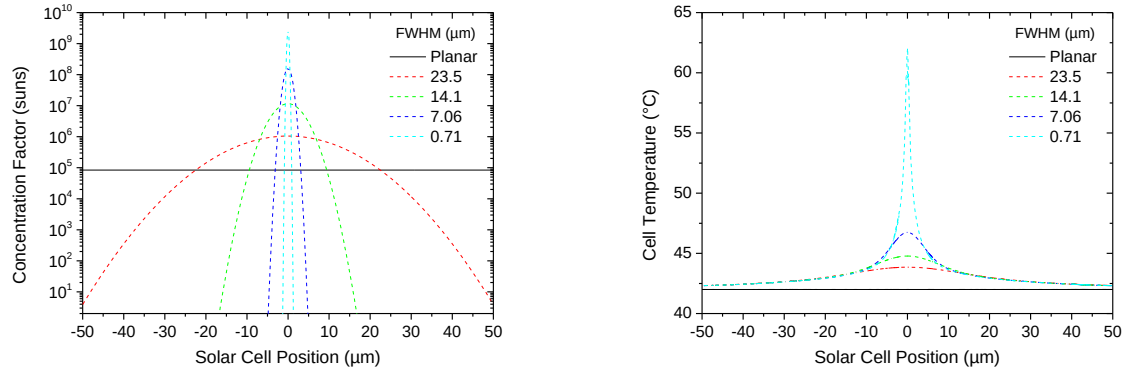

c)

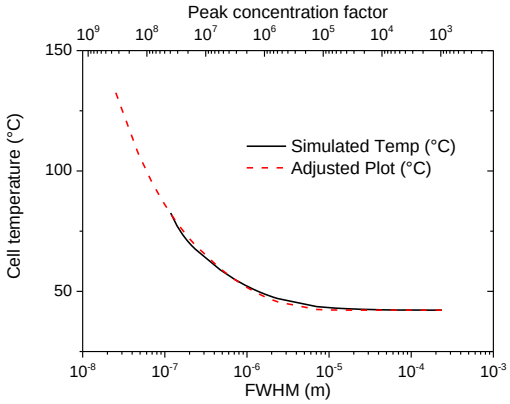

Figure 6: (a) Input Gaussian beams, **(b)** surface temperature profile along the solar cell surface as a function of the incident Gaussian beam profile and **(c)** simulated temperature distribution and a fitting plot for different Gaussian irradiation profiles applied on the realistic solar cell structure for the device structure: a 3 mm thick glass substrate (with an area of 1 mm^2), an 800 nm molybdenum layer (with an area of 1 mm^2), a 2 μm thick CIGSe absorber, a 50 nm thick buffer layer (CdS), a 450 nm thick transparent conductive layer (AZO) and 1 mm thick glass upperstrate (with an area of 1 mm^2).

The temperature behavior under different Gaussian irradiation distributions was studied and the maximum values are illustrated in figure 6c. This performance is fitted using equation 7, which shows a good agreement with the simulation. The formula used to fit the simulated maximum cell temperature as a function of the incident Gaussian beam profile is:

$$T_{under\ Gaussian\ Beam} = T_{Flat\ Beam} \cdot \left[1 + e^{-\frac{3}{2}} \cdot \frac{e^{-\sigma}}{\sqrt{\sigma}} \right] \qquad [7]$$

where $T_{Flat\ Beam}$ is the solar cell temperature for a uniform beam, and σ represents the standard deviation (Gaussian RMS width expressed in μm, value applied in equation without

units). Narrow spot beams cannot be seen by the dense mesh matrix in our simulation model because of the limited RAM memory resources [32]. Therefore, FWHM values below 500 nm cannot be studied and are neglected in our simulations. Nevertheless, assuming that equation 7 follows the temperature behavior of the cell for narrow Gaussian beams, profiles with a FWHM lower than $4 \cdot 10^{-2}$ μm are expected to produce localized temperatures higher than 150°C. Hence, for a standard deviation below 0.017 μm the stability of the solar cell is uncertain what could lead to a shunted cell. A FWHM above $4 \cdot 10^{-2}$ μm will provide the best thermal performance when a CIGSe solar cell is illuminated with a Gaussian beam.

4. Conclusions

Heat dissipation and cell temperature have demonstrated a high impact on the design of CPV systems. Micrometer-sized CIGSe solar cells offer improved heat dissipation presenting a good disposition to enhance efficiency and boost the performance of the cell by concentrating light on it. According to our thermal studies, parameters as the back contact material or thickness have minor contributions to heat dissipation, although back contact size presents an important functionality to reduce the solar cell temperature. Our finite element method simulations have demonstrated that high concentration factors, up to 10^5x, are feasible to be applied on micro CIGSe solar cells (PV cell width of 20 μm for a 3 mm wide substrate and down to 3.2 μm for a 0.5 mm wide substrate). Below this value, the PV device has a temperature under the pn-junction breakdown range.

Homogeneous irradiation profiles are desirables to decrease the cell temperature under concentration. However, in order to reduce operational requirements like tracking, spectral tolerances or lens misalignment, a Gaussian beam shape could be used to reduce the device requirements leading to a cheaper CPV technology. Gaussian illumination profiles lead to a localized temperature increment on the solar cell; even though, for FWHM values above $4 \cdot 10^{-2}$ μm the cell temperature is in a trustworthy range.

Further analysis will prove the benefits of these thermal studies including an opto-electronic model, where j-V simulations under concentrated light will be investigated for different scenarios.

5. Acknowledgements

The authors would like to thank the funding from the Helmholtz-Association for Young Investigator groups within the Initiative and Networking fund (VH-NG-928). The research leading to these results has received funding from the European Union Seventh Framework Programme (FP7/2007-2013) under Grant Agreement n° 609788. We are grateful to all the advice provided by our colleagues from Helmholtz-Zentrum Berlin, special thanks to R. Klenk, P. Manley, G. Mangalgiri and W. Raja. M.-Ch. Lux-Steiner is acknowledged for introducing the topic of CIGSe micro concentrators.

6. References

[1] ZSW, "ZSW Sets New World Record for Thin-film Solar," [Online]. Available: https://www.zsw-bw.de/fileadmin/user_upload/PDFs/Pressemitteilungen/2016/pr09-2016-ZSW-WorldRecordCIGS.pdf.

[2] Shogo Ishizuka et al., "Buried p-n junction formation in $CuGaSe_2$ thin-film solar cells," *Applied Physics Letters 104, 031606 (2014); doi: 10.1063/1.4861858.*

[3] Su-Huai Wei et al., "Effects of Ga addition to $CuInSe_2$ on its electronic, structural, and defect properties," *Applied Physics Letters 72, 3199 (1998); doi: 10.1063/1.121548.*

[4] Albert Polman et al., "Photonic design principles for ultrahigh-efficiency photovoltaics," *Nature Materials 11, 174–177 (2012), doi:10.1038/nmat3263.*

[5] Guanchao Yin et al., "Integration of plasmonic Ag nanoparticles as a back reflector in ultra-thin $Cu(In,Ga)Se_2$ solar cells," *Applied Surface Science, Volume 355, 15 November 2015, Pages 800–804.*

[6] Myriam Paire et al., "Toward microscale $Cu(In,Ga)Se_2$ solar cells for efficient conversion and optimized material usage: Theoretical evaluation," *Applied Physics, American Institute of Physics, 2010, 108, pp.034907, http://dx.doi.org/10.1063/1.3460629.*

[7] Myriam Paire et al., "Microscale solar cells for high concentration on polycrystalline $Cu(In,Ga)Se_2$ thin films," *Appl. Phys. Lett. 98, 264102 (2011); http://dx.doi.org/10.1063/1.3604789.*

[8] Sebastien Jutteau et al., "Study of a micro-CPV system based on $Cu(In,Ga)Se_2$ microcells array," *Applied Optics, http://dx.doi.org/10.1364/AO.99.099999.*

[9] Bernhard Reinhold et al., "Monolithically interconnected lamellar $Cu(In,Ga)Se_2$ micro solar cells under full white light concentration," *Progress in Photovoltaics: Research and Applications (2015), doi: 10.1002/pip.2611.*

[10] Erwin Lotter et al., "Identification of loss mechanism in CIGS micro-cells for concentrator applications," *32nd European Photovoltaic Solar Energy Conference and Exhibition (2016).*

[11] Gerhard Peharz et al., "Investigations on the temperature dependence of CPV modules equipped with triple-junction solar cells," *Prog. Photovolt: Res. Appl. 2011; 19:54–60, doi: 10.1002/pip.987.*

[12] Sascha Sadewasser et al., "Materials efficient deposition and heat management of $CuInSe_2$ microconcentrator solar cells," *Solar Energy Materials & Solar Cells 159 (2017) 496–502. http://dx.doi.org/10.1016/j.solmat.2016.09.041.*

[13] COMSOL Multiphysics, Finite element analysis, solver and simulation software , [Online].

Available: https://www.comsol.com/.

[14] Avancis, "PowerMax® Premium class solar module," [Online]. Available: http://www.avancis.de/en/products/powermaxr/.

[15] John H. Scofield et al, "Sputtered Molybdenum Bilayer Back Contact for Copper Indium Diselenide-Based," *Thin Solid Films, 260 (1), pp. 26-31 (May 1, 1995).*

[16] H.A. Al-Thani et al., "The Effect of Mo Back Contact on Na Out-Diffusion and Device Performance of Mo/Cu(In,Ga)Se_2/CdS/ZnO Solar Cells," *29th IEEE PV Specialists Conference (2002).*

[17] Ju-Heon Yoon et al., "Effect of a Mo back contact on Na diffusion in CIGS thin film solar cells," *Prog. Photovolt: Res. Appl. 2013; 21:58–63, DOI: 10.1002/pip.2193.*

[18] Manz GmbH, "CIGS MODULES & BIPV: High-performance CIGS thin-film solar modules and building-integrated photovoltaics from the CISGinnoline".

[19] A. Luque, Cu(In,Ga)Se_2 Solar Cells, in Handbook of Photovoltaic Science and Engineering, John Wiley & Sons, Ltd, Chichester, UK (2003). doi: 10.1002/0470014008.ch13.

[20] AZoM, "AZoNetwork UK Ltd," [Online]. Available: http://www.azom.com/.

[21] The Engineering Toolbox, [Online]. Available: http://www.engineeringtoolbox.com/convective-heat-transfer-d_430.html.

[22] COMSOL Multiphysics, "Heat Transfer Module, User´s Guide".

[23] Stefan Puttnins, "Breakdown characteristics of flexible Cu(In,Ga)Se_2 solar cells," *Solar Energy Materials & SolarCells 120 (2014) 506–511, doi: 10.1016/j.solmat.2013.09.031.*

[24] Priyanka Singh et al., "Temperature dependence of solar cell performance — an analysis," *Solar Energy Materials & Solar Cells 101 (2012) 36–45, doi:10.1016/j.solmat.2012.02.019.*

[25] J.L. Johnson et al., "Effects of 2nd Phases, Stress, and Na at the Mo/Cu_2ZnSnS_4 Interface," *MRS Proceedings, 1268 (2010). doi: 10.1557/PROC-1268-EE03-03..*

[26] K. Orgassa et al., "Alternative back contact materials for thin film Cu(In,Ga)Se_2 solar cells," *Thin Solid Films 431 –432 (2003) 387–391.*

[27] British Geological Survey, "Risk list 2015 - Current supply risk for chemical elements or element group which are of economic value," [Online]. Available: http://www.bgs.ac.uk/mineralsuk/statistics/risklist.html.

[28] Katie Shanks et al., "Optics for concentrating photovoltaics: Trends, limits and opportunities for materials and design," *Renewable and Sustainable Energy Reviews 60 (2016) 394–407, http://dx.doi.org/10.1016/j.rser.2016.01.089.*

[29] Fraunhofer ISE and NREL, "Current status of concentrator photovoltaics (CPV) technology," [Online]. Available: www.ise.fraunhofer.de/en/renewable-energy-data.

[30] Linak, "Improving energy efficiency," [Online]. Available: http://www.linak.com/techline/?id3=2236.

[31] David C. Miller et al., "Durability of Fresnel lenses: A review specific to the concentrating photovoltaic application," *Solar Energy Materials & Solar Cells 95 (2011) 2037–2068, doi:10.1016/j.solmat.2011.01.031.*

[32] HZB (EE-NOPT group), "Supernano computer details: Intel(R) Xeon(R) CPU E5-2650 v2 @ 2.60Ghz (2 processors) 128 GB RAM".

[33] Fredrik Rostvall, "Potential Induced Degradation of CIGS Solar Cells," Uppsala Universitet, 2014.